Ecotoxicology and Environmental Safety 208 (2021) 111735

Contents lists available at ScienceDirect

Ecotoxicology and Environmental Safety

journal homepage: www.elsevier.com/locate/ecoenv

Research paper

Reductive transformation of hexavalent chromium by ferrous ions in a frozen environment: Mechanism, kinetics, and environmental implications

Quoc Anh Nguyen [a,b], Bomi Kim [a,b], Hyun Young Chung [a,b], Anh Quoc Khuong Nguyen [c], Jungwon Kim [d,*], Kitae Kim [a,b,**]

[a] Korea Polar Research Institute (KOPRI), Incheon 21990, Republic of Korea
[b] Department of Polar Sciences, University of Science and Technology (UST), Incheon 21990, Republic of Korea
[c] Department of Chemistry, Hallym University, Chuncheon, Gangwon-do 24252, Republic of Korea
[d] Department of Environmental Sciences and Biotechnology, Hallym University, Chuncheon, Gangwon-do 24252, Republic of Korea

ARTICLE INFO

Editor by: Professor Bing Yan

Keywords:
Ice chemistry
Hexavalent chromium
Ferrous ion
Natural detoxification
Cr^{6+}-contaminated wastewater

ABSTRACT

The transformation between hexavalent chromium (Cr^{6+}) and trivalent chromium (Cr^{3+}) has a significant impact on ecosystems, as Cr^{6+} has higher levels of toxicity than Cr^{3+}. In this regard, a variety of Cr^{6+} reduction processes occurring in natural environments have been studied extensively. In this work, we investigate the reductive transformation of Cr^{6+} by ferrous ions (Fe^{2+}) in ice at −20 °C, and compare the same process in water at 25 °C. The Fe^{2+}-mediated reduction of Cr^{6+} occurred much faster in ice than it did in water. The accelerated reduction of Cr^{6+} in ice is primarily ascribed to the accumulation of Cr^{6+}, Fe^{2+}, and protons in the grain boundaries formed during freezing, which constitutes favorable conditions for redox reactions between Cr^{6+} and Fe^{2+}. This freeze concentration phenomenon was verified using UV–visible spectroscopy with *o*-cresolsulfonephthalein (as a pH indicator) and confocal Raman spectroscopy. The reductive transformation of Cr^{6+} (20 μM) by Fe^{2+} in ice proceeded rapidly under various Fe^{2+} concentrations (20–140 μM), pH values (2.0–5.0), and freezing temperatures (–10 to −30 °C) with a constant molar ratio of oxidized Fe^{2+} to reduced Cr^{6+} (3:1). This result implies that the proposed mechanism (i.e., the redox reaction between Cr^{6+} and Fe^{2+} in ice) can significantly contribute to the natural conversion of Cr^{6+} in cold regions. The Fe^{2+}-mediated Cr^{6+} reduction kinetics in frozen Cr^{6+}-contaminated wastewater was similar to that in frozen Cr^{6+} solution. This indicates that the variety of substrates typically present in electroplating wastewater have a negligible effect on the redox reaction between Cr^{6+} and Fe^{2+} in ice; it also proposes that the Fe^{2+}/freezing process can be used for the treatment of Cr^{6+}-contaminated wastewater.

1. Introduction

Chromium (Cr) is one of the most ubiquitous pollutants, occurring in a number of environments including soil, surface water, and groundwater (Coetzee et al., 2020; Daneshvar et al., 2019). Hexavalent Cr (Cr^{6+}) and trivalent Cr (Cr^{3+}) are frequently found among various Cr species; Cr^{6+} is considered more dangerous than Cr^{3+}, as a result of its higher toxicity and rates of mobility (Costa, 2003; Zhu et al., 2019). Cr^{6+} pollution is a product of both anthropogenic and natural processes. It has been reported that wastewater containing Cr^{6+}, produced from various industries such as electroplating, wood treatment, and leather tanning, is occasionally discharged into natural environments without proper treatment (Pakade et al., 2019; Shi et al., 2020). As for natural processes, Cr is present predominantly in the form of Cr^{3+} in natural minerals (Barnhart, 1997; Morrison et al., 2015). However Cr^{3+}, which is released from Cr-bearing minerals through weathering and dissolution, is readily converted to Cr^{6+} by various natural oxidants, such as manganese oxides (Mn_2O_3 and MnO_2) (Hausladen and Fendorf, 2017), oxygen (O_2) (Panichev et al., 2008), and hydrogen peroxide (H_2O_2) (Luo and Chatterjee, 2010). In addition, the presence of Mn^{2+}-oxidizing bacteria (e.g., *Bacillus* sp. strain SG-1), which are found in almost all environments, accelerates the oxidative transformation of Cr^{3+} to Cr^{6+} (Murray and Tebo, 2007).

The natural reduction of Cr^{6+} to Cr^{3+} is also possible through both

* Corresponding author.
** Corresponding author at: Korea Polar Research Institute (KOPRI), Incheon 21990, Republic of Korea.
E-mail addresses: jwk@hallym.ac.kr (J. Kim), ktkim@kopri.re.kr (K. Kim).

https://doi.org/10.1016/j.ecoenv.2020.111735
Received 20 October 2020; Received in revised form 24 November 2020; Accepted 25 November 2020
Available online 4 December 2020

chemical and biological processes. This behavior significantly reduces the toxicity and potential risk of Cr^{6+}. Cr^{6+} reduction by iron (e.g., ferrous (Fe^{2+})-ferric (Fe^{3+}) oxyhydroxides (Bond and Fendorf, 2003), Fe^{2+}-bearing minerals (Anderson et al., 1994), and Fe^{2+} ions (Anderson et al., 1994; Fendorf and Li, 1996; Li et al., 2020; Monček ová et al., 2016)) has been investigated. A variety of organic compounds, such as oxalic acid, α-carbonyl carboxylic acids, α-hydroxyl carboxylic acids, and substituted phenols, can act as reductants for Cr^{6+} (Deng and Stone, 1996). Additionally, Cr^{6+} can be reduced to Cr^{3+} by hydrogen sulfide (H_2S) (Kim et al., 2001), which is abundant in marine environments. It has been also reported that the biological reduction of Cr^{6+} occurs directly within cells in the absence of oxygen, while biologically formed reactive oxygen species are primarily involved in the Cr^{6+} reduction process when oxygen is present (Pradhan et al., 2017). Among these Cr^{6+} reduction processes, the Fe^{2+}-mediated reduction of Cr^{6+} accounts for a significant portion of natural Cr^{6+} reduction as Fe^{2+} is abundant, particularly under suboxic and acidic conditions (Lau et al., 2015). In addition, Fe^{2+} can be produced through the photochemical reactions of Fe^{3+} and iron oxides, even in the presence of oxygen (Lueder et al., 2020; Walte and Morel, 1984). The concentrations of Fe^{2+} in water reached millimolar levels in specific geographic areas (Chen et al., 2010; Davison and Seed, 1983; Heaney and Davison, 1977).

Although most chemical reactions proceed more slowly at lower temperatures, several chemical reactions, such as the reductive dissolution of metal oxides (e.g., manganese oxide and iron oxide) (Jeong et al., 2015; Kim et al., 2012), the formation of molecular iodine (or tri-iodide) from iodate (or iodide) (Kim et al., 2016, 2019a), and the transformation of bromate to organobromine compounds in the presence of humic substances (Hao et al., 2020), proceed more rapidly when the aqueous solutions are frozen. These unique chemical reactions that disobey the Arrhenius rule are likely due to the freeze concentration phenomenon, which is induced during the freezing process. Although frozen solutions appear to be in all-solid state, they contain a small quantity of liquid in the regions between ice crystals, which are usually referred to as ice grain boundaries or liquid brines. The freeze concentration phenomenon indicates the accumulation of solutes and protons (under acidic conditions) in the ice grain boundaries, via exclusion from ice crystals during the freezing process (O'Concubhair and Sodeau, 2013). The freeze concentration phenomenon gradually increases as the size of ice crystals increases (i.e., as the volume of ice grain boundaries decreases). If the degree of freeze concentration-induced positive effect is higher than the degree of the negative effect induced by the temperature decrease, the chemical reactions occurring within the ice proceed more rapidly than they would in water.

In addition to natural Cr^{6+} reduction processes in water and soil, the reduction of Cr^{6+} in ice (more precisely frozen Cr^{6+} solution) has been recently investigated in order to better understand the fate and behavior of Cr^{6+} in cold areas, such as polar regions, high-latitude areas, and mid-latitude areas in winter. It has been reported that the reduction of Cr^{6+} by H_2O_2 (Kim et al., 2015), 4-chlorophenol (Ju et al., 2017), and nitrite (NO_2^-) (Kim et al., 2017) is enhanced when these aqueous solutions are frozen. However, the kinetics and mechanism of Cr^{6+} reduction by Fe^{2+} in ice have not yet been investigated despite the significant contribution of Fe^{2+} to natural Cr^{6+} reduction processes in water and soil. In this study, we investigate the reductive transformation of Cr^{6+} by Fe^{2+} in ice (i.e., at temperatures below the freezing point) in comparison with the same process in water (i.e., at temperatures above the freezing point). The effects of various experimental parameters on Cr^{6+} reduction kinetics in ice are examined. In addition, the reductive transformation of Cr^{6+} by Fe^{2+} in ice was monitored in situ, and its mechanism is discussed in detail. Finally, Cr^{6+} reduction experiments were performed using Cr^{6+}-contaminated wastewater, with the purpose of verifying the practical application of the Fe^{2+}/freezing process for the treatment of Cr^{6+}-contaminated wastewater.

2. Chemicals and methods

2.1. Chemicals

From Sigma-Aldrich, we purchased sodium dichromate dihydrate ($Na_2Cr_2O_7{\cdot}2H_2O$, Cr^{6+}, ≥99.5%), iron(II) sulfate heptahydrate ($FeSO_4{\cdot}7H_2O$, Fe^{2+}, ≥99.0%), sulfuric acid (H_2SO_4, ≥95.0%), 1,5-diphenylcarbazide ($C_{13}H_{14}N_4O$, DPC, ≥99.95%), 1,10-phenanthroline ($C_{12}H_8N_2$, ≥99%), ammonium acetate ($C_2H_7NO_2$, ≥98%), perchloric acid ($HClO_4$, 60%), sodium hydroxide (NaOH, 1 M), and *o*-cresolsulfonephthalein sodium salt ($C_{21}H_{17}NaO_5S$, CR, ≥95%). Acetone (C_3H_6O, ≥99.5%) was purchased from Junsei Chemical. All solutions were prepared using deionized water (R ≥ 18.0 MΩ·cm) produced using a Barnstead water purification system (Milli-Q Direct 16). Cr^{6+}-contaminated wastewater was originated from an electroplating factory (Busan, Republic of Korea), and used as an alternative source of Cr^{6+} without further purification.

2.2. Experimental procedure

The experimental solutions were prepared by adding aliquots of chemical stock solutions to water in a 100-mL volumetric flask (usually $[Cr^{6+}]$ = 20 μM and $[Fe^{2+}]$ = 70 μM). The solutions were initially adjusted to the desired pH values (usually pH 4.0) using an $HClO_4$ or NaOH solution. A total of 5 mL of solution were placed in a 15-mL polypropylene conical tube (Falcon). This conical tube, which contained Cr^{6+} and Fe^{2+}, was immersed in a temperature-controlled bath to induce chemical reactions at the desired temperatures (usually −20 °C and 25 °C for the reactions in ice and water, respectively). Ethanol was used as a temperature control medium, and its temperature was set to the desired value prior to immersion of the conical tube into the temperature-controlled bath. For the ice phase reaction, the reaction time was measured from the moment of immersion in the temperature-controlled bath. For the aqueous phase reaction, the reaction time began when the pH adjustment was complete. The conical tubes were withdrawn from the temperature-controlled bath at predetermined time intervals and then placed in a beaker containing lukewarm water (35 °C) for 1 min, in order to thaw the frozen samples. The aqueous samples were also placed in a beaker containing lukewarm water for 1 min, prior to analysis. All experiments were performed in triplicate, and the average values with standard deviations are presented.

2.3. Chemical analyses

The concentrations of Cr^{6+} and Fe^{2+} were measured using the colorimetric 1,5-diphenylcarbazide (DPC) (Rice et al., 2017) and 1, 10-phenanthroline methods (Stucki and Anderson, 1981), respectively. To determine the Cr^{6+} concentration, DPC reagent solution was prepared by adding DPC (0.05 g) to the mixture of acetone (25 mL) and sulfuric acid (0.25 mL), and 0.1 mL of DPC reagent solution was added into a 15-mL conical tube containing 2.9 mL of dilute aqueous sample (0.5 mL of sample + 2.4 mL water). To determine the Fe^{2+} concentration, 1.5 mL of 1,10-phenanthroline solution (2 g/L) and 1.5 mL of ammonium acetate (0.1 M) were added to a 15-mL conical tube containing 2 mL of the aqueous sample. The conical tubes were mixed vigorously using a vortexer and maintained for 1 h in the dark prior to analysis. The mixed samples were transferred from the conical tubes to a 3-mL cuvette. The absorbance of the samples was measured at 510 nm for Fe^{2+} analysis and 540 nm for Cr^{6+} analysis, using a UV–visible spectrophotometer (Shimadzu UV-2600). The calibration curves of Fe^{2+} ($r^2 = 0.9998$) and Cr^{6+} ($r^2 = 0.9999$) were used to convert the measured absorbance values to the concentrations of Fe^{2+} and Cr^{6+}.

The pH of the frozen sample (more precisely the ice grain boundary region) was estimated by measuring the UV–visible absorption spectra of *o*-cresolsulfonephthalein (CR) (Krausková et al., 2016; Vetráková et al., 2017), which exhibits different maximum absorption wavelengths

(λ_{max}) depending on pH. An aqueous solution containing Cr^{6+}, Fe^{2+}, and CR (3 mL) was added into a 4-mL rectangular cuvette and then frozen at −20 °C in a temperature-controlled bath. The rectangular cuvette containing the frozen sample was withdrawn from the temperature-controlled bath after 1 h, and its UV–visible absorption spectra were recorded using a UV–visible spectrophotometer (Shimadzu UV-2600) without melting. The UV–visible absorption spectra were referenced against a frozen pure water sample.

The change in Cr^{6+} concentration in the ice grain boundary region of the frozen sample was investigated in situ (i.e., without melting) using a confocal Raman spectroscope (Renishaw inVia Qontor) combined with a temperature-controlled microscope stage (Linkam Scientific THMS600). An aqueous sample containing Cr^{6+} and Fe^{2+} (0.1 mL) was loaded onto the sample holder mounted on the temperature-controlled stage. The temperature decreased from 0 to −40 °C at a rate of −2.0 °C/min. The local concentration of Cr^{6+} in the frozen sample (i.e., the Cr^{6+} concentration distribution image) was obtained by measuring the intensity of the characteristic Raman Cr^{6+} peak at 852 cm^{-1}. A monochromatic 532 nm laser was employed as the excitation source.

3. Results and discussion

3.1. Reductive transformation of Cr^{6+} by Fe^{2+} in water and ice

The reductive transformation of Cr^{6+} by Fe^{2+} in ice at −20 °C was measured and compared with the same process in water at 25 °C under the following conditions: $[Cr^{6+}]$ = 20 μM, $[Fe^{2+}]$ = 70 μM, and pH 4.0 (Fig. 1). In the presence of Fe^{2+}, the concentration of Cr^{6+} in the water slowly decreased with the reaction time, but did not reach zero even after 24 h. However, the reduction of Cr^{6+} proceeded very rapidly in the ice, and was almost complete after 30 min (Fig. 1a). In accordance with the Cr^{6+} reduction trend, the oxidation of Fe^{2+} in ice was much more significant than the same process in water (Fig. 1b). These results indicate that the redox reaction between Cr^{6+} and Fe^{2+} is favored in the ice phase in contrast to the aqueous phase. The reduction of Cr^{6+} in the absence of Fe^{2+} and the oxidation of Fe^{2+} in the absence of Cr^{6+} were minimal in both water and ice. Therefore, the proton-mediated reduction of Cr^{6+} (Chaudhary et al., 2003) and oxygen-mediated oxidation of Fe^{2+} (Iwai et al., 1982) can be ignored under the experimental conditions identical to those shown in Fig. 1. In other words, Fe^{2+} can be considered as a primary reductant for Cr^{6+} and vice versa (reaction (1), which was obtained from the reduction reactions of $HCr^{(6+)}O_4^-/Cr^{3+}$ (reaction (2)) and Fe^{3+}/Fe^{2+} (reaction (3))). To be more concrete, Fe^{2+} ions form inner-sphere complexes with Cr^{6+} ions and protons (reaction (4)), and the inner-sphere complexes ($Fe^{(2+)}H_2Cr^{(6+)}O_4^{2+}$) are decomposed to Fe^{3+} ions and Cr^{5+} species ($H_3Cr^{(5+)}O_4$) by protons (reaction (5)). The resulting Cr^{5+} species are subsequently reduced to Cr^{4+} and Cr^{3+} species by Fe^{2+} ions (Espenson, 1970; Sedlack and Chan, 1997).

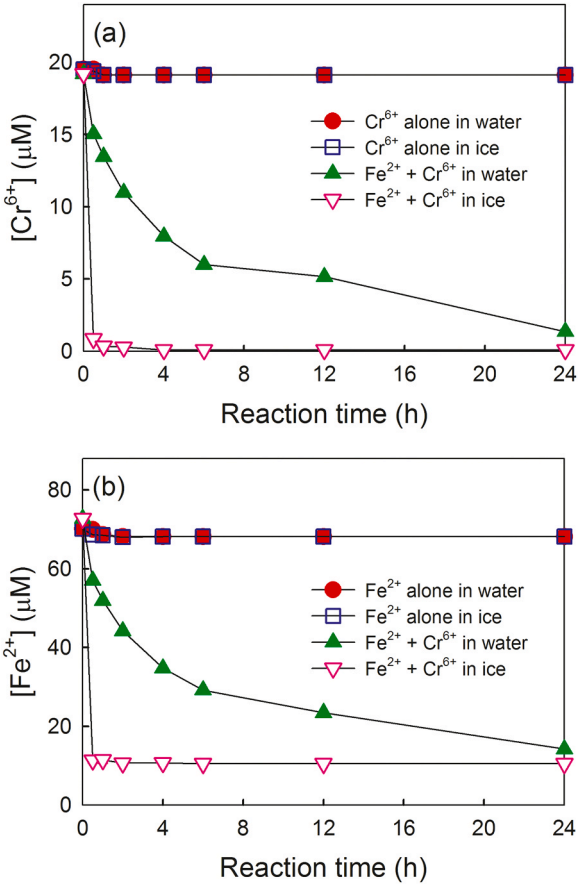

Fig. 1. (a) Reduction of Cr^{6+} by Fe^{2+} and (b) oxidation of Fe^{2+} by Cr^{6+} in water and ice. Experimental conditions: reaction temperature = 25 °C or −20 °C, $[Cr^{6+}]$ = 20 μM, $[Fe^{2+}]$ = 70 μM, and pH 4.0.

$$3Fe^{2+}+HCr^{(6+)}O_4^-+7\ H^+ \rightarrow 3Fe^{3+}+Cr^{3+}+4\ H_2O \quad (1)$$

$$HCr^{(6+)}O_4^-+7\ H^+ +3e^- \rightarrow Cr^{3+}+4\ H_2O \quad (2)$$

$$Fe^{3+}+e^- \rightarrow Fe^{2+} \quad (3)$$

$$Fe^{2+}+HCr^{(6+)}O_4^-+H^+ \rightarrow Fe^{(2+)}H_2Cr^{(6+)}O_4^{2+} \quad (4)$$

$$Fe^{(2+)}H_2Cr^{(6+)}O_4^{2+}+H^+ \rightarrow Fe^{3+}+H_3Cr^{(5+)}O_4 \quad (5)$$

According to reaction (1), it takes three Fe^{2+} ions to reduce one Cr^{6+} ion. 61 μM of Fe^{2+} were oxidized while at the same time, 20 μM of Cr^{6+} were reduced after 1 h in ice (Fig. 1). This experimental molar ratio of oxidized Fe^{2+} to reduced Cr^{6+} (3.05:1) is closely matched to the theoretical molar ratio (3.0:1). Therefore, reaction (1) is presumed to be the primary redox reaction pathway between Cr^{6+} and Fe^{2+} in ice.

3.2. Freeze concentration phenomenon

The reductive transformation of Cr^{6+} by Fe^{2+} is favored at higher Fe^{2+} concentrations and more acidic conditions according to reaction (1). It has been reported that the concentrations of solutes and protons (under acidic conditions) in an aqueous solution are significantly increased by freezing, because they are excluded from the ice crystals (solid phase) and are instead located within the ice grain boundaries (liquid phase) (Heger et al., 2005, 2006). Therefore, the freeze concentration phenomenon that occurs during freezing is most likely responsible for the accelerated reduction of Cr^{6+} in the presence of Fe^{2+} in ice.

The accumulation and reduction of Cr^{6+} in ice grain boundaries after freezing were monitored in situ using a confocal Raman spectroscope combined with a temperature-controlled microscope stage (Fig. 2). The aqueous solution containing Cr^{6+} and Fe^{2+} at pH 3.0 was frozen for 20 min, and the change in Cr^{6+} concentration was monitored as a function of reaction time. The frozen solution was rigidly compartmentalized into two regions: the ice grain boundary region and the ice crystal region. The size of the ice grain boundaries (a few μm) was much smaller than that of ice crystals (dozens ~ hundreds of μm) (Fig. 2a).

Most Cr^{6+} ions exist as H_2CrO_4, $HCrO_4^-$, CrO_4^{2-}, and $Cr_2O_7^{2-}$ in aqueous solutions, and their molar ratios depend on the Cr^{6+} concentration and pH. These Cr^{6+} species exhibit characteristic Raman peaks in the range of 800–1000 cm^{-1}, which are assigned to Cr–O stretching modes (Hardcastle and Wachs, 1988). The local concentrations of Cr^{6+} in frozen solution (i.e., in ice grain boundary and ice crystal regions) were obtained by comparing the Raman intensities at 852 cm^{-1}; the results are shown using a rainbow scale from red (high concentration) to violet (low concentration). The red color in the ice grain boundary region and

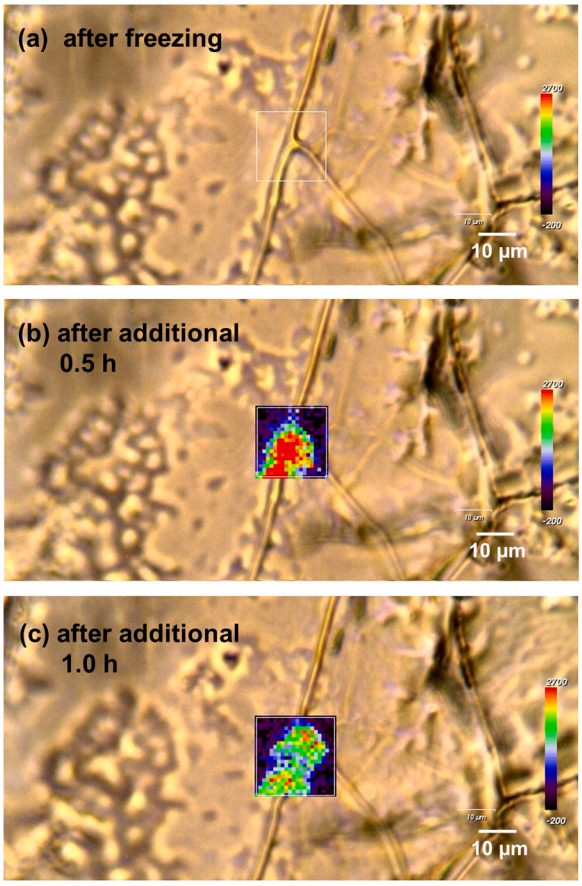

Fig. 2. (a) Optical image of the frozen solution containing Cr^{6+} and Fe^{2+}. Local concentrations of Cr^{6+} in the frozen solution after additional time: (b) 0.5 h and (c) 1.0 h. Experimental conditions: $[Cr^{6+}] = 1$ mM, $[Fe^{2+}] = 1$ mM, and pH 3.0. For part a, the temperature decreased from 0 to −40 °C at a rate of −2.0 °C/min. For parts b and c, the temperature was maintained at −40 °C.

violet color in the ice crystal region clearly indicate that most Cr^{6+} ions exist within the ice grain boundaries after freezing (Fig. 2b). The color in the ice grain boundary region changed from red to green after an additional 0.5 h of reaction in the frozen state (Fig. 2b vs. Fig. 2c). This result confirms that the reductive transformation of Cr^{6+} by Fe^{2+} in a frozen solution occurs within the ice grain boundaries.

In order to confirm the decrease in the pH of aqueous solutions containing Cr^{6+} and Fe^{2+} and, if so, quantitatively assess the value of the decrease in pH by freezing, the spectrophotometric method using *o*-cresolsulfonephthalein (CR) as a pH indicator was employed (Krausková et al., 2016; Vetráková et al., 2017) (Fig. 3). The maximum absorption wavelength (λ_{max}) of CR changes depending on the pH of the solution, through protonation and deprotonation (i.e., the λ_{max} of singly protonated CR (434 nm) (Rottman et al., 1999) is red-shifted by acidification (by 84 nm) and basification (by 139 nm)) (Krausková et al., 2016; Vetráková et al., 2017). In an aqueous solution containing Cr^{6+} and Fe^{2+} at pH 4.0, only one absorption band at 434 nm appeared, because almost 100% of CR exists in a singly protonated form (λ_{max} = 434 nm) at pH 4.0. When the aqueous solution was frozen, two absorption bands at 434 nm and 518 nm were observed. The doubly protonated CR exhibits λ_{max} at 518 nm (Rottman et al., 1999). Therefore, the generation of the absorption band at 518 nm with a decrease in the absorption band at 434 nm after freezing implies that singly protonated CR molecules are transformed into doubly protonated CR molecules in ice via pH decrease.

The ratio of [singly protonated CR] to [doubly protonated CR] in the

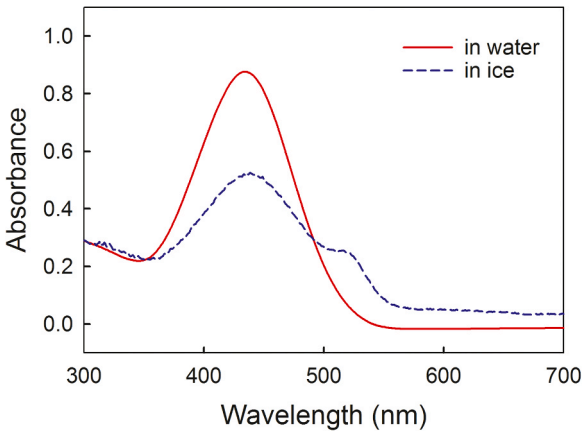

Fig. 3. Change of UV–visible absorption spectra of CR after freezing. Experimental conditions: freezing temperature = –20 °C, freezing time = 1 h, $[Cr^{6+}]$ = 20 μM, $[Fe^{2+}]$ = 70 μM, [CR] = 6.7 μM, and pH 4.0.

frozen solution (Fig. 3) was determined via the non-negative least squares minimization (Kim et al., 2019a), and the result was approximately 6.02. The pH value of the frozen solution was calculated by substituting the ratio of [singly protonated CR] to [doubly protonated CR] (6.02) in the Henderson-Hasselbalch equation ($pH = pK_{a1} + \log$ ([singly protonated CR]/[doubly protonated CR]), where $pK_{a1} = 1.10$ (Dean, 1992)). The calculated pH of the frozen solution was approximately 1.88 when the aqueous solution of Cr^{6+} (20 μM) and Fe^{2+} (70 μM) at pH 4.0 was frozen at −20 °C. Although the degree of pH decrease after freezing can be influenced by the concentrations of Cr^{6+} and Fe^{2+}, pH in aqueous solution, freezing temperature, and freezing rate, it is obvious that freezing constitutes favorable conditions for Fe^{2+}-mediated Cr^{6+} reduction by decreasing the pH under acidic conditions.

To investigate the influence of the freeze concentration phenomenon (i.e., the accumulation of Fe^{2+} and protons in the ice grain boundaries) on the reduction kinetics of Cr^{6+}, the concentrations of reduced Cr^{6+} in water after 2 h were measured at $[Cr^{6+}]$ = 20 μM, $[Fe^{2+}]$ = 70 or 700 μM, and pH 2.0, 3.0, or 4.0, and the results were compared (Fig. 4).

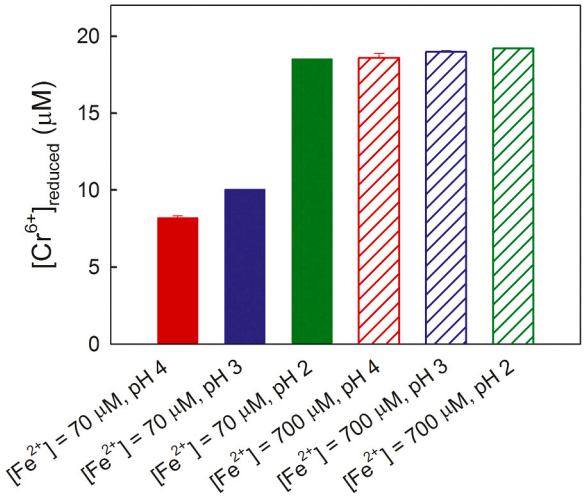

Fig. 4. Effects of Fe^{2+} concentration increase and/or pH decrease on the Fe^{2+}-mediated reduction of Cr^{6+} in water. Experimental conditions: reaction temperature = 25 °C, reaction time = 2 h, $[Cr^{6+}]$ = 20 μM, $[Fe^{2+}]$ = 70 or 700 μM, and pH = 2.0, 3.0, or 4.0.

The reduction of Cr^{6+} increased with increasing concentration of Fe^{2+} at the same pH and decreasing pH at the same Fe^{2+} concentration. Importantly, the increase in Fe^{2+} concentration and the decrease in pH synergistically accelerated the Fe^{2+}-mediated Cr^{6+} reduction. These behaviors indicate that the freeze concentrations of Cr^{6+}, Fe^{2+}, and protons in the ice grain boundaries, as demonstrated by the confocal Raman spectroscopy and pH estimation using CR (Figs. 2 and 3), are the primary reasons for the acceleration of the Fe^{2+}-mediated Cr^{6+} reduction in ice.

3.3. Impact of various factors on the redox conversion between Cr^{6+} and Fe^{2+}

The effects of Fe^{2+} concentration, pH, and freezing temperature on the reductive transformation of Cr^{6+} by Fe^{2+} in ice were measured and compared with those in water. In addition, the oxidative transformation of Fe^{2+} after the chemical reaction with Cr^{6+} was also monitored (Fig. 5). The results were expressed in terms of the concentrations of reduced Cr^{6+} and oxidized Fe^{2+} after 0.5 h. The reduction of Cr^{6+} was enhanced with increasing Fe^{2+} concentration in both water and ice. However, the Fe^{2+}-mediated reduction of Cr^{6+} in ice was much higher than that in water, in all Fe^{2+} concentrations tested ($[Fe^{2+}]$ = 20–140 μM) (Fig. 5a). In accordance with this higher reduction of Cr^{6+} in ice, the oxidation of Fe^{2+} by Cr^{6+} was more significant in ice (Fig. 5b). This result demonstrates that in a broad range of Fe^{2+} concentrations, the redox conversion between Cr^{6+} and Fe^{2+} in ice proceeds more rapidly than it does in water.

Fig. 5c and d show the pH-dependent Cr^{6+} reduction by Fe^{2+} and Fe^{2+} oxidation by Cr^{6+} in water and ice. Both the reduction of Cr^{6+} (Fig. 5c) and oxidation of Fe^{2+} (Fig. 5d) increased with decreasing pH in both phases. These results confirm that the concentration of protons is a key factor in determining the efficiency of Cr^{6+} reduction by Fe^{2+}. The reduction of Cr^{6+} accompanied the oxidation of Fe^{2+} sharply decreased with increasing pH in water (16.5 μM at pH 2.0, 7.2 μM at pH 3.0, 4.1 μM at pH 4.0, and 2.0 μM at pH 5.0). However, the effect of pH on Cr^{6+} reduction (also Fe^{2+} oxidation) was relatively minor in ice, under a pH range of 2.0–5.0. Complete reduction (20 μM) of Cr^{6+} was observed at pH 2.0 and 3.0 in ice. 18.3 μM and 16.0 μM of Cr^{6+} were reduced in

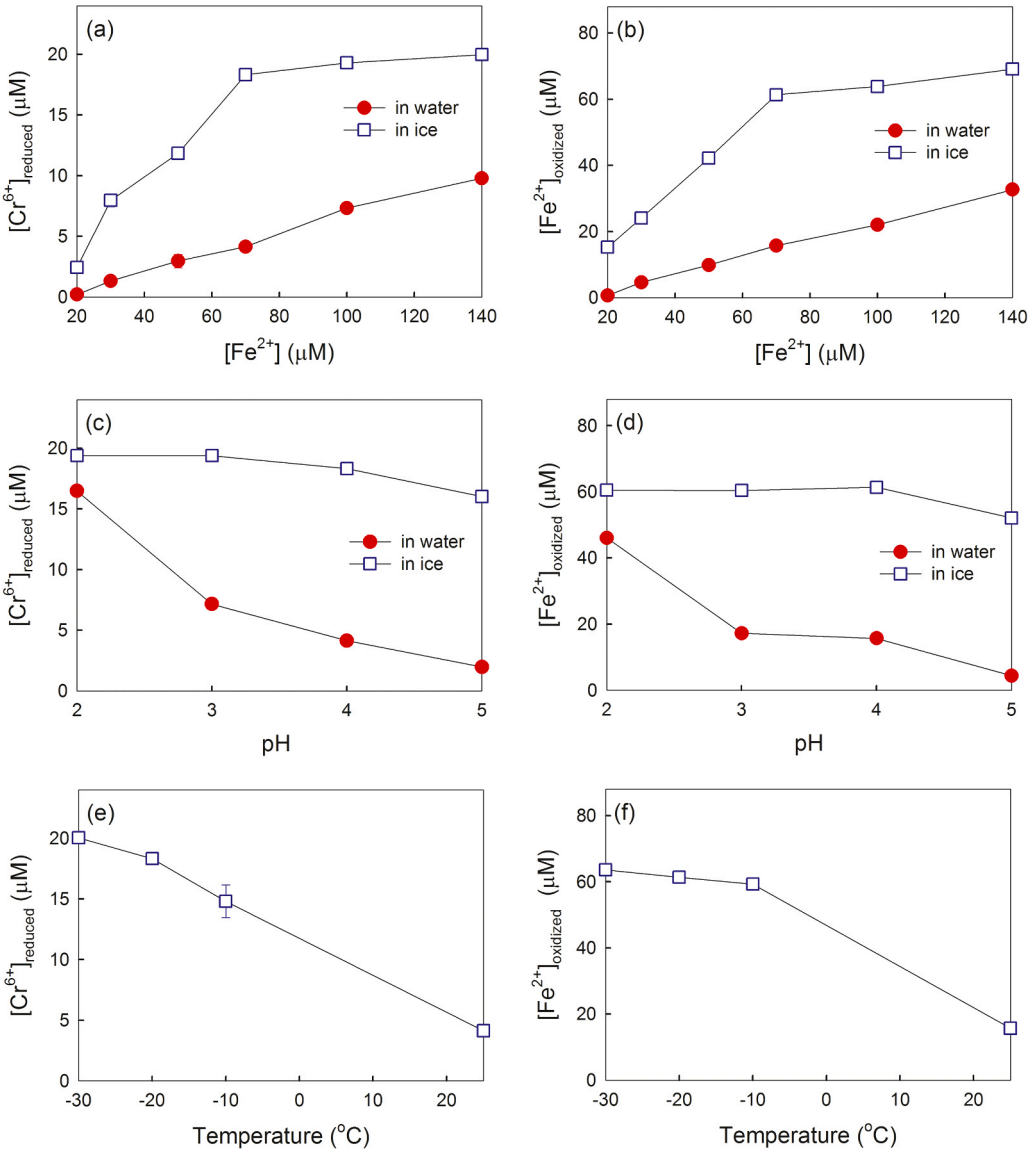

Fig. 5. Effects of (a and b) Fe^{2+} concentration, (c and d) pH, and (e and f) temperature on the redox reaction between Cr^{6+} and Fe^{2+} in water and ice. Experimental conditions: $[Cr^{6+}]$ = 20 μM, $[Fe^{2+}]$ = 70 μM in the cases of c–f, pH 4.0 in the cases of a–b and e–f, reaction temperature = 25 °C or −20 °C in the cases of a–d, and reaction time = 0.5 h.

ice at pH 4.0 and 5.0, respectively. This result indicates that the freezing-induced acceleration of Cr^{6+} reduction in the presence of Fe^{2+} is not restricted to extremely acidic conditions and can also occur under mild acidic conditions.

The effect of freezing temperature on the redox reaction between Cr^{6+} and Fe^{2+} was also investigated (Fig. 5e and f). The reduction of Cr^{6+} (Fig. 5e) and oxidation of Fe^{2+} (Fig. 5f) increased as the freezing temperature decreased, within a temperature range of –10 to −30 °C. This behavior can be explained by the degree of the freeze concentration phenomenon depending on the freezing temperature. Specifically, ice crystals grow faster at lower freezing temperatures, which induces a faster decline in the volume of ice grain boundaries. If the volume of the ice grain boundaries is smaller, then the concentrations of Cr^{6+}, Fe^{2+}, and protons in the ice grain boundaries are higher (i.e., the degree of freeze concentration phenomenon is higher). These relationships among the freezing temperature, the volume of ice grain boundaries, and the degree of freeze concentration phenomenon help to explain why the Fe^{2+}-mediated Cr^{6+} reduction in ice is more significant at lower freezing temperatures with the same Fe^{2+} and Cr^{6+} concentrations and pH.

3.4. Environmental relevance and practical application

Because both Cr^{6+} and Fe^{2+} are widely distributed across a variety of environments, they inevitably coexist in many geographic areas. It has been recently reported that the concentrations of Cr in high-latitude areas and polar regions have increased due to long-range transport from mid-latitude areas (Kozak et al., 2016; Weinbruch et al., 2012). In addition, a field experiment performed in the Arctic regions showed that Fe^{2+} ions are produced from the photochemical reaction of iron oxides under polar conditions (Kim et al., 2010, 2019b). Therefore, the redox reaction between Cr^{6+} and Fe^{2+} in ice can significantly contribute to the natural detoxification of Cr^{6+} in cold regions, such as high-latitude areas and polar regions. Acid mine drainage (AMD) contains a variety of metals, including high concentrations of Cr and Fe (Luo et al., 2020; RoyChowdhury et al., 2019). Cr^{6+} and Fe^{2+} released from AMD into the environment in mid-latitude areas during the winter season can undergo a redox reaction between Cr^{6+} and Fe^{2+} in ice, which can reduce the potential risks of Cr^{6+} to humans and ecological systems in a short time.

From a practical point of view, the Fe^{2+}/freezing process can be applied to the remediation of Cr^{6+}-contaminated wastewater. We tested the reductive transformation of Cr^{6+} by Fe^{2+} in ice using Cr^{6+}-contaminated wastewater obtained from an electroplating factory (Fig. 6). The chemical composition of the electroplating wastewater is listed in Table 1. The wastewater was mixed with Fe^{2+} solution, the pH was adjusted to 4.0, and the mixture was frozen. Despite the presence of a variety of substrates in electroplating wastewater, such as K, Fe, Ca, Cu, Na, As, B, Al, Mg, Mo, Pb, and Tl, the Cr^{6+} reduction kinetics in the electroplating wastewater at pH 4.0 was similar to that in the Cr^{6+} solution at pH 4.0. The Fe^{2+} oxidation kinetics was also little affected by the additional substrates present in the electroplating wastewater. The preferential reactivity of Cr^{6+} toward Fe^{2+} in ice, even in the presence of other substrates, makes the Fe^{2+}/freezing process an efficient alternative for the treatment of Cr^{6+}-contaminated wastewater. Because most Cr^{6+}-contaminated wastewater is already highly acidic (Bankole et al., 2019; Bokare and Choi, 2010), the addition of acid is not necessary. The initial pH of the mixture containing the electroplating wastewater ($[Cr^{6+}]$ = 20 μM) and Fe^{2+} (70 μM) was 4.5. When the mixture of wastewater and Fe^{2+} was frozen without acidification, the reductive transformation of Cr^{6+} by Fe^{2+} was significant and comparable to that of the acidified mixture.

4. Conclusions

We investigated the reductive transformation of Cr^{6+} by Fe^{2+} in ice (i.e., after freezing) and water (i.e., without freezing), and compared the results between the two. The Fe^{2+}-mediated reduction of Cr^{6+} was significantly accelerated by freezing. The accelerated Cr^{6+} reduction in the presence of Fe^{2+} in ice is primarily ascribed to the accumulation of Cr^{6+}, Fe^{2+}, and protons in the ice grain boundaries, which constitutes favorable conditions for the redox reaction between Cr^{6+} and Fe^{2+} (i.e., low pH and high solute concentration). The experimental molar ratios of oxidized Fe^{2+} to reduced Cr^{6+} in the ice were similar to the theoretical value (3:1), regardless of Fe^{2+} concentration, pH, freezing temperature, and the presence of other substrates. The Fe^{2+}-mediated Cr^{6+} reduction in ice proceeded rapidly under mild acidic conditions, which are frequently found in natural environments. Therefore, redox reactions between Fe^{2+} and Cr^{6+} occurring in a frozen state can play important roles in the Cr^{6+} detoxification process in nature. In addition, the Fe^{2+}/freezing process can be used for the removal of Cr^{6+} in Cr^{6+}-contaminated wastewater. If this process is operated in cold regions, electrical energy for freezing is not required; thus, this strategy would make the Fe^{2+}/freezing process for Cr^{6+} reduction economically feasible. A cost comparison between the conventional Cr^{6+}-contaminated wastewater treatment process and the Fe^{2+}/freezing process is very difficult at this stage, because the reduction efficiency and cost significantly vary depending on the type and volume of Cr^{6+}-contaminated wastewater. For the exact economic evaluation of the Fe^{2+}/freezing process, many reduction experiments under different freezing systems and experimental conditions with a pilot experiment should be performed; this can be investigated in further studies.

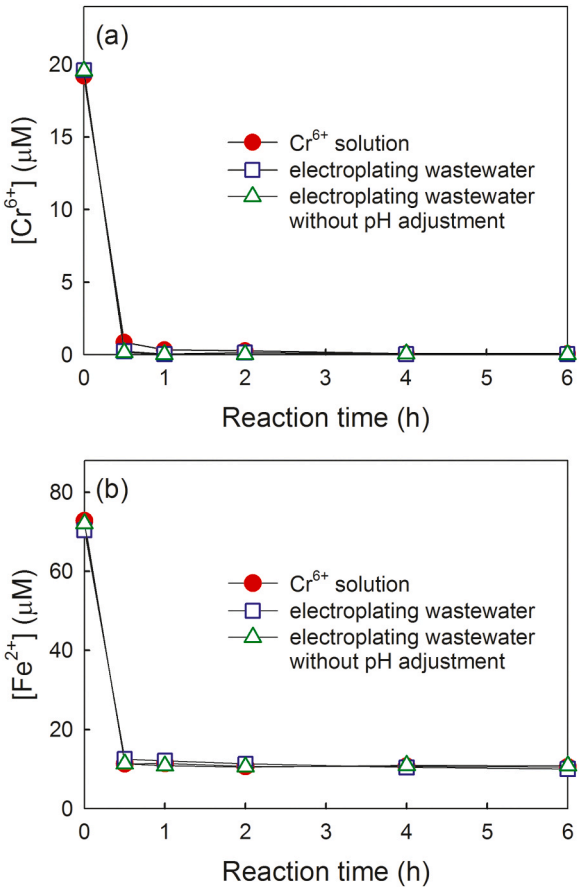

Fig. 6. Time profiles of (a) Cr^{6+} and (b) Fe^{2+} concentrations in electroplating wastewater and Cr^{6+} solution during the freezing process. Experimental conditions: reaction temperature = –20 °C, $[Cr^{6+}]$ = 20 μM, $[Fe^{2+}]$ = 70 μM, and pH 4.0 (with pH adjustment) or 4.5 (without pH adjustment).

Table 1
Chemical composition of Cr^{6+}-contaminated wastewater originated from an electroplating factory.

type	Cr	K	Fe	Ca	Cu	Na	As	B	Al	Mg	Mo	Pb	Tl
concentration (ppm)	36451	6247	541	286	235	185	93	63	54	53	52	48	28

Inductively coupled plasma-optical emission spectroscopy (Thermo iCAP 6300 Duo) was used for the analysis of Cr^{6+}-contaminated wastewater.

CRediT authorship contribution statement

Quoc Anh Nguyen: Investigation, Writing - original draft, Writing - review & editing. **Bomi Kim:** Formal analysis, Writing - review & editing. **Hyun Young Chung:** Investigation, Writing - review & editing. **Anh Quoc Khuong Nguyen:** Writing - review & editing. **Jungwon Kim:** Conceptualization, Visualization, Writing - original draft, Writing - review & editing, Supervision, Project administration, Funding acquisition. **Kitae Kim:** Conceptualization, Visualization, Writing - original draft, Writing - review & editing, Supervision, Project administration, Funding acquisition.

Declaration of Competing Interest

The authors declare that they have no known competing financial interests or personal relationships that could have appeared to influence the work reported in this paper.

Acknowledgments

This research was supported by the Korea Polar Research Institute (KOPRI) project (PE20030) and the Hallym University Research Fund (HRF-202002-010).

References

Anderson, L.D., Kent, D.B., Davis, J.A., 1994. Batch experiments characterizing the reduction of Cr(VI) using suboxic material from a mildly reducing sand and gravel aquife. Environ. Sci. Technol. 28, 178–185.
Bankole, M.T., Abdulkareem, A.S., Mohammed, I.A., Ochigbo, S.S., Tijani, J.O., Abubakre, O.K., Roos, W.D., 2019. Selected heavy metals removal from electroplating wastewater by purified and polyhydroxylbutyrate functionalized carbon nanotubes adsorbents. Sci. Rep. 9, 4475.
Barnhart, J., 1997. Occurrences, uses, and properties of chromium. Regul. Toxicol. Pharmacol. 26, S3–S7.
Bokare, A.D., Choi, W., 2010. Chromate-induced activation of hydrogen peroxide for oxidative degradation of aqueous organic pollutants. Environ. Sci. Technol. 44, 7232–7237.
Bond, D.L., Fendorf, S., 2003. Kinetics and structural constraints of chromate reduction by green rusts. Environ. Sci. Technol. 37, 2750–2757.
Chaudhary, A.J., Goswami, N.C., Grimes, S.M., 2003. Electrolytic removal of hexavalent chromium from aqueous solutions. J. Chem. Technol. Biotechnol. 78, 877–883.
Chen, K.-F., Kao, C.-M., Chen, C.-W., Surampalli, R.Y., Lee, M.-S., 2010. Control of petroleum-hydrocarbon contaminated groundwater by intrinsic and enhanced bioremediation. J. Environ. Sci. 22, 864–871.
Coetzee, J.J., Bansal, N., Chirwa, E.M.N., 2020. Chromium in environment, its toxic effect from chromite-mining and ferrochrome industries, and its possible bioremediation. Expo. Health 12, 51–62.
Costa, M., 2003. Potential hazards of hexavalent chromate in our drinking water. Toxicol. Appl. Pharmacol. 188, 1–5.
Daneshvar, E., Zarrinmehr, M.J., Kousha, M., Hashtjin, A.M., Saratale, G.D., Maiti, A., Vithanage, M., Bhatnagar, A., 2019. Hexavalent chromium removal from water by microalgal-based materials: adsorption, desorption and recovery studies. Bioresour. Technol. 293, 122064.
Davison, W., Seed, G., 1983. The kinetics of the oxidation of ferrous iron in synthetic and natural waters. Geochim. Cosmochim. Acta 47, 67–79.
Dean, J.A., 1992. Lange's Handbook of Chemistry, 14th ed. McGraw-Hill, New York.
Deng, B., Stone, A.T., 1996. Surface-catalyzed chromium(VI) reduction: reactivity comparisons of different organic reductants and different oxide surfaces. Environ. Sci. Technol. 30, 2484–2494.
Espenson, J.H., 1970. Rate studies on the primary step of the reduction of chromium (VI) by iron (II). J. Am. Chem. Soc. 92, 1880–1883.
Fendorf, S.E., Li, G., 1996. Kinetics of chromate reduction by ferrous iron. Environ. Sci. Technol. 30, 1614–1617.
Hao, Z., Shi, F., Cao, D., Liu, J., Jiang, G., 2020. Freezing-induced bromate reduction by dissolved organic matter and the formation of organobromine compounds. Environ. Sci. Technol. 54, 1668–1676.
Hardcastle, F.D., Wachs, I.E., 1988. Raman spectroscopy of chromium oxide supported on Al_2O_3, TiO_2 and SiO_2: a comparative study. J. Mol. Catal. 46, 173–186.
Hausladen, D.M., Fendorf, S., 2017. Hexavalent chromium generation within naturally structured soils and sediments. Environ. Sci. Technol. 51, 2058–2067.
Heaney, S.I., Davison, W., 1977. The determination of ferrous iron in natural waters with 2,2' bipyridyl. Limnol. Oceanogr. 22, 753–760.
Heger, D., Jirkovský, J., Klán, P., 2005. Aggregation of methylene blue in frozen aqueous solutions studied by absorption spectroscopy. J. Phys. Chem. A 109, 6702–6709.
Heger, D., Klánová, J., Klán, P., 2006. Enhanced protonation of cresol red in acidic aqueous solutions caused by freezing. J. Phys. Chem. B 110, 1277–1287.
Iwai, M., Majima, H., Awakura, Y., 1982. Oxidation of Fe (II) in sulfuric acid solutions with dissolved molecular oxygen. Metall. Trans. B 13, 311–318.
Jeong, D., Kim, K., Min, D.W., Choi, W., 2015. Freezing-enhanced dissolution of iron oxides: effects of inorganic acid anions. Environ. Sci. Technol. 49, 12816–12822.
Ju, J., Kim, J., Vetráková, Ľ., Seo, J., Heger, D., Lee, C., Yoon, H.-I., Kim, K., Kim, J., 2017. Accelerated redox reaction between chromate and phenolic pollutants during freezing. J. Hazard. Mater. 329, 330–338.
Kim, C., Zhou, Q., Deng, B., Thornton, E.C., Xu, H., 2001. Chromium(VI) reduction by hydrogen sulfide in aqueous media: stoichiometry and kinetics. Environ. Sci. Technol. 35, 2219–2225.
Kim, K., Choi, W., Hoffmann, M.R., Yoon, H.-I., Park, B.-K., 2010. Photoreductive dissolution of iron oxides trapped in ice and its environmental implications. Environ. Sci. Technol. 44, 4142–4148.
Kim, K., Yoon, H.-I., Choi, W., 2012. Enhanced dissolution of manganese oxide in ice compared to aqueous phase under illuminated and dark conditions. Environ. Sci. Technol. 46, 13160–13166.
Kim, K., Ju, J., Kim, B., Chung, H.Y., Vetráková, Ľ., Heger, D., Saiz-Lopez, A., Choi, W., Kim, J., 2019. Nitrite-induced activation of iodate into molecular iodine in frozen solution. Environ. Sci. Technol. 53, 4892–4900.
Kim, K., Kim, J., Bokare, A.D., Choi, W., Yoon, H.-I., Kim, J., 2015. Enhanced removal of hexavalent chromium in the presence of H_2O_2 in frozen aqueous solutions. Environ. Sci. Technol. 49, 10937–10944.
Kim, K., Menacherry, S.P.M., Kim, J., Chung, H.Y., Jeong, D., Saiz-Lopez, A., Choi, W., 2019b. Simultaneous and synergic production of bioavailable iron and reactive iodine species in ice. Environ. Sci. Technol. 53, 7355–7362.
Kim, K., Yabushita, A., Okumura, M., Saiz-Lopez, A., Cuevas, C.A., Blaszczak-Boxe, C.S., Min, D.W., Yoon, H.-I., Choi, W., 2016. Production of molecular iodine and tri-iodide in the frozen solution of iodide: implication for polar atmosphere. Environ. Sci. Technol. 50, 1280–1287.
Kim, K., Chung, H.Y., Ju, J., Kim, J., 2017. Freezing-enhanced reduction of chromate by nitrite. Sci. Total Environ. 590–591, 107–113.
Kozak, K., Polkowska, Ż., Stachnik, Ł., Luks, B., Chmiel, S., Ruman, M., Lech, D., Kozioł, K., Tsakovski, S., Simeonov, V., 2016. Arctic catchment as a sensitive indicator of the environmental changes: distribution and migration of metals (Svalbard). Int. J. Environ. Sci. Technol. 13, 2779–2796.
Krausková, Ľ., Procházková, J., Klašková, M., Filipová, L., Chaloupková, R., Malý, S., Damborský, J., Heger, D., 2016. Suppression of protein inactivation during freezing by minimizing pH changes using ionic cryoprotectants. Int. J. Pharm. 509, 41–49.
Lau, C.K.Y., Krewulak, K.D., Vogel, H.J., 2015. Bacterial ferrous iron transport: the Feo system. FEMS Microbiol. Rev. 40, 273–298.
Li, X., He, X., Wang, H., Liu, Y., 2020. Characteristics and long-term effects of stabilized nanoscale ferrous sulfide immobilized hexavalent chromium in soil. J. Hazard. Mater. 389, 122089.
Lueder, U., Jørgensen, B.B., Kappler, A., Schmidt, C., 2020. Fe(III) photoreduction producing Fe^{2+}_{aq} in oxic freshwater sediment. Environ. Sci. Technol. 54, 862–869.
Luo, C., Routh, J., Dario, M., Sarkar, S., Wei, L., Luo, D., Liu, Y., 2020. Distribution and mobilization of heavy metals at an acid mine drainage affected region in South China, a post-remediation study. Sci. Total Environ. 724, 138122.
Luo, Z., Chatterjee, N., 2010. Kinetics of oxidation of Cr(III)-organic complexes by H_2O_2. Chem. Speciat. Bioavailab. 22, 25–34.
Mončeková, M., Novotný, R., Koplík, J., Kalina, L., Bílek, V., Šoukal, F., 2016. Hexavalent chromium reduction by ferrous sulphate heptahydrate addition into the Portland clinker. Procedia Eng. 151, 73–79.
Morrison, J.M., Goldhaber, M.B., Mills, C.T., Breit, G.N., Hooper, R.L., Holloway, J.M., Diehl, S.F., Ranville, J.F., 2015. Weathering and transport of chromium and nickel from serpentinite in the Coast Range ophiolite to the Sacramento Valley, California, USA. Appl. Geochem. 61, 72–86.
Murray, K.J., Tebo, B.M., 2007. Cr(III) is indirectly oxidized by the Mn(II)-oxidizing bacterium *Bacillus* sp. Strain SG-1. Environ. Sci. Technol. 41, 528–533.
O'Concubhair, R., Sodeau, J.R., 2013. The effect of freezing on reactions with environmental impact. Acc. Chem. Res. 46, 2716–2724.
Pakade, V.E., Tavengwa, N.T., Madikizela, L.M., 2019. Recent advances in hexavalent chromium removal from aqueous solutions by adsorptive methods. RSC Adv. 9, 26142–26164.
Panichev, N., Mabasa, W., Ngobeni, P., Mandiwana, K., Panicheva, S., 2008. The oxidation of Cr(III) to Cr(VI) in the environment by atmospheric oxygen during the bush fires. J. Hazard. Mater. 153, 937–941.

Pradhan, D., Sukla, L.B., Sawyer, M., Rahman, P.K.S.M., 2017. Recent bioreduction of hexavalent chromium in wastewater treatment: a review. J. Ind. Eng. Chem. 55, 1–20.

Rice, E.W., Baird, R.B., Eaton, A.D., 2017. Standard Methods for the Examination of Water and Wastewater, 23rd ed. American Public Health Association, American Water Works Association, and Water Environment Federation.

Rottman, C., Grader, G., Hazan, Y.D., Melchior, S., Avnir, D., 1999. Surfactant-induced modification of dopants reactivity in sol-gel matrixes. J. Am. Chem. Soc. 121, 8533–8543.

RoyChowdhury, A., Sarkar, D., Datta, R., 2019. Removal of acidity and metals from acid mine drainage-impacted water using industrial byproducts. Environ. Manag. 63, 148–158.

Sedlack, D.L., Chan, P.G., 1997. Reduction of hexavalent chromium by ferrous iron. Geochim. Cosmochim. Acta 61, 2185–2192.

Shi, J., McGill, W.B., Chen, N., Rutherford, P.M., Whitcombe, T.W., Zhang, W., 2020. Formation and immobilization of Cr(VI) species in long-term tannery waste contaminated soils. Environ. Sci. Technol. 54, 7226–7235.

Stucki, J.W., Anderson, W.L., 1981. The quantitative assay of minerals for Fe^{2+} and Fe^{3+} using 1,10-phenanthroline 1. Sources of variability. Soil Sci. Soc. Am. J. 45, 633–637.

Vetráková, Ľ., Vykoukal, V., Heger, D., 2017. Comparing the acidities of aqueous, frozen, and freeze-dried phosphate buffers: is there a “pH memory” effect? Int. J. Pharm. 530, 316–325.

Walte, T.D., Morel, F.M.M., 1984. Photoreductive dissolution of colloidal iron oxides in natural waters. Environ. Sci. Technol. 18, 860–868.

Weinbruch, S., Wiesemann, D., Ebert, M., Schütze, K., Kallenborn, R., Ström, J., 2012. Chemical composition and sources of aerosol particles at Zeppelin Mountain (Ny Ålesund, Svalbard): an electron microscopy study. Atmos. Environ. 49, 142–150.

Zhu, Y., Yan, J., Xia, L., Zhang, X., Luo, L., 2019. Mechanisms of Cr(VI) reduction by *Bacillus* sp. CRB-1, a novel Cr(VI)-reducing bacterium isolated from tannery activated sludge. Ecotoxicol. Environ. Saf. 186, 109792.